International Journal of Advances in Applied Sciences (IJAAS)
Vol. 15, No. 2, June 2026, pp. 861~871
ISSN: 2252-8814, DOI: 10.11591/ijaas.v15.i2.pp861-871

Numerical comparison of mathematical modeling approaches on the performances of link coupling beams

Musbar, Hanif, Khairul Miswar
Department of Civil Engineering, Politeknik Negeri Lhokseumawe, Lhokseumawe, Indonesia

Article Info

Article history:

Received Mar 13, 2025
Revised Apr 20, 2026
Accepted May 23, 2026

Keywords:

Behavior
Link coupling beams
Mathematical models
Performance
Plasticity

ABSTRACT

The precision of inelastic steel-link response predictions in eccentrically braced frames (EBFs) is contingent on the material model employed. In the absence of comprehensive guidelines concerning constitutive choices for long-link coupling beams (LCBs), this study undertakes a comparative analysis of four models through nonlinear finite element simulations of three American Institute of Steel Construction (AISC) 341-22–compliant specimens under cyclic loading conditions in Ansys. Two mathematical formulations (Ramberg–Osgood and Kaufmann cyclic) and two plasticity-based formulations (multilinear kinematic hardening and isotropic hardening) were evaluated for shear strength, overstrength, and plastic rotation capacity. Mathematical models consistently generate stable hysteresis with uniform stiffness degradation, while plasticity-based models exhibit greater variability. It was observed that all specimens exceeded the nominal shear strength of 271.98 kN, attaining peak strengths of 350.72–391.86 kN (overstrength 1.29–1.44). The plastic rotations range from 0.039 to 0.051 rad, which exceeds the minimum requirement of 0.02 rad for long links. The Kaufmann cyclic model, when combined with multilinear kinematic hardening, has been shown to optimally reproduce key EBF hysteretic behavior. This advancement in model selection for numerical assessment and improvement in seismic performance predictions in performance-based design is a significant contribution to the field.

Corresponding Author:

Musbar
Department of Civil Engineering, Politeknik Negeri Lhokseumawe
Lhokseumawe, Indonesia
Email: musbaribrahim@pnl.ac.id

1. INTRODUCTION

In eccentrically braced frames (EBFs), the link element dissipates seismic energy through localized yielding, preserving global structural integrity. The yielding mechanism—shear or flexure—depends on link length, with the link rotation angle governing elastic and inelastic response. Per American Institute of Steel Construction (AISC)/American National Standards Institute (ANSI) 341-22 [1], required rotation capacities vary with the link length ratio (ρ): short links ($\rho<1.6$) require 0.08 rad; intermediate links ($1.6\leq\rho\leq2.6$) require 0.02–0.08 rad; and long links ($2.6<\rho\leq5$) require 0.02 rad. Intermediate and long links, essential for layouts with large architectural openings, must satisfy enhanced performance criteria, including inelastic rotation limits [1]. Compared to short links, intermediate and long links exhibit inferior energy dissipation and deformation capacity under cyclic loading, and have therefore received less research attention. Nevertheless, they are widely used in configurations requiring wider spans or greater spatial flexibility. Recent studies aim to improve their performance by mitigating local buckling and fracture through end-region stiffening ahead of panel zone connections to redistribute stress concentrations. Additionally, replaceable links have emerged

as a cost-effective strategy for seismic regions, enabling post-earthquake replacement of damaged components. This approach enhances structural resilience and facilitates rapid recovery, reducing downtime and maintenance costs [2].

Research on the concept of using replaceable links in EBF structures was introduced in the early 2000s. This concept has become very realistic and effective to be applied to EBF structures with construction sites located in seismic zones. In the 20 years since its introduction, research on replaceable links has continued to develop. Research development on this concept includes numerical and experimental analysis of the performance improvement of replaceable links in EBFs, namely; the relationship between the link and the coupling beam [3]–[5], the review of the gusset brace at the ends and the center of the link [6]–[8], investigation using a tapered hollow box in accordance with the requirements of the AISC/ANSI 341-16 standard [9]–[11]. Study of replaceable corrugated steel links and replaceable shear links [12], [13]. The results of a study conducted by Li [14] on the K-configuration of EBFs showed that the seismic demand on beams and braces is highly related to the link overstrength of the corresponding story. By reducing the span and using high-strength steel, the ductility and ultimate load capacity of the EBF Y-configuration structure were significantly improved [15]. The research with the Y-configuration on the replaceable link on EBFs with cyclic load shows a stable hysteretic response and high energy dissipation on the device [16], [17]. Research on the development of cast steel replaceable links for EBFs [18]. Research on the seismic behavior of removable links in EBFs with semirigid connections and damage analysis of replaceable links [19], [20].

Replaceable link coupling beams (LCBs) are proposed to improve the seismic resilience of EBFs by enabling wider openings and simpler post-earthquake retrofitting. This study employs nonlinear finite element analysis to compare constitutive models for the cyclic response of long-LCBs. Low-cycle uniaxial tension–compression loading is simulated to capture nonlinear material behavior (including Bauschinger effects and ratcheting) and local web/flange buckling. By quantifying shear strength, overstrength, stiffness degradation, energy dissipation, and plastic rotation, model performance and long-link capacity are assessed. In conventional AISC 341-22 long links, plastic deformation concentrates near the beam ends; the LCB configuration is designed to delay such end-localization and improve ductility. The LCB concept also supports sustainable construction (e.g., reuse of steel elements) and is straightforward to implement in earthquake-prone regions. The structural configurations and yielding mechanisms of the investigated EBF systems are illustrated in Figure 1. Figures 1(a) and 1(b) present the conventional long-link and LCB-link configurations, respectively. The corresponding yielding mechanisms are shown in Figures 1(c) and 1(d). In the conventional long-link system, inelastic deformation is concentrated within the link region, which serves as the primary energy dissipation component. In contrast, the LCB-link configuration is intended to improve the distribution of stresses and plastic deformation while preserving the desired ductile response. The comparison between these configurations provides the basis for evaluating the effectiveness of the proposed LCB system in enhancing cyclic performance and energy dissipation capacity.

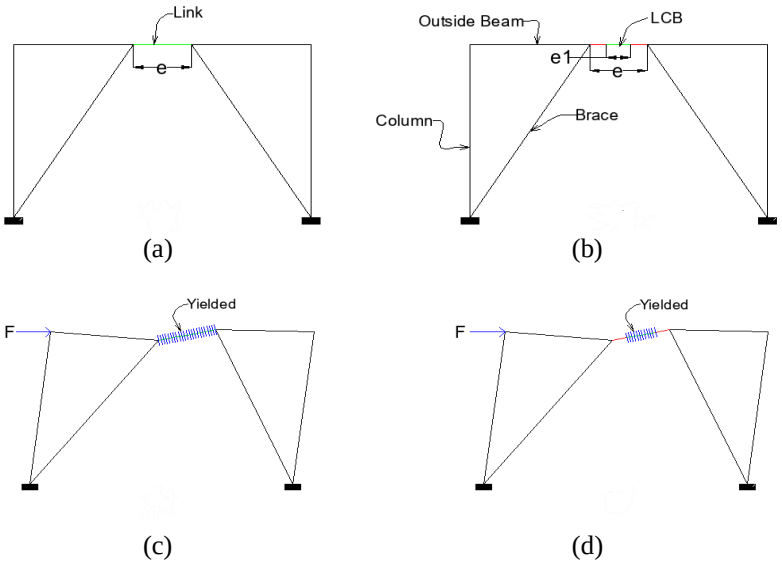

Figure 1. Structural configurations and yielding mechanisms of EBF systems: (a) conventional long link configurations, (b) LCB link configurations, (c) yielding mechanism of conventional long link, and (d) yielding mechanism of LCB link [21]

2. METHOD

An attempt is made to improve the performance of long links by extending the outside beam beyond the panel zone toward the initial long link. The beam extension can behave as a coupling beam. Between the coupling beams are link elements with smaller cross-section sizes than the coupling beams. Based on the link length, the link at the center between the coupling beams is designed as a short link. The change in profile of the long link with the combination link of the coupling beam and the short link between the coupling beams is called the LCB system [21].

2.1. Mathematical model of stress-strain curve

The stress-strain curve obtained from monotonic loading tensile test of wide flange (WF) steel profiles is called the engineering stress-strain curve; then, the curve is modeled into a true stress-strain curve model, called the true stress-strain curve. Several methods are used to model the stress-strain curve into a nonlinear material model, including power functions, Ramberg-Osgood, and Menegotto-Pinto. Numerical analysis for the test piece model uses stress-strain data from steel tensile tests under monotonic loading with a mathematical model of the stress-strain curve by Ramberg-Osgood. The study also used a mathematical model of the stress-strain curve based on the approach of cyclic force test results from the research of Kaufmann. The application of hardening models to monotonic and cyclic tensile test data of structural steel demonstrates notable variations in the predicted strength behavior of the specimens [22]. The material properties of the WF profile steel from the steel tensile test are shown in Table 1. The nonlinear stress–strain behavior of steel was represented using the Ramberg–Osgood and Kauffman models. As shown in Figure 2, separate stress–strain relationships were developed for the flange and web components to capture their mechanical response under loading. Figure 2(a) presents the stress–strain model for flange, while Figure 2(b) shows the corresponding model for web.

Table 1. Material properties of steel from the results of tensile test

Section	F_y (MPa)	F_u (MPa)	ε_y (mm/mm)	ε_u (mm/mm)	Elong (%)
Web	487.64	595.61	0.0027	0.1166	16.05
Flange	401.45	540.08	0.0019	0.1721	24.55

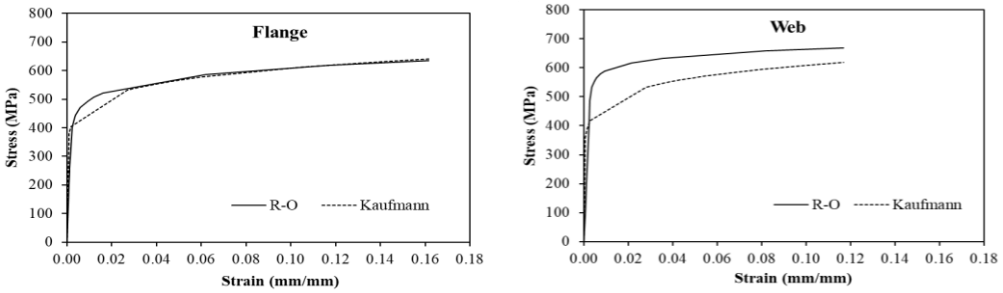

(a) (b)

Figure 2. Mathematical models of stress–strain curves based on the Ramberg–Osgood and Kauffman methods: (a) flange and (b) web [23]

2.2. Plasticity models

In the field of material science, the study of material behavior and the factors that contribute to failure in structures is of great interest. One particular area of study is the phenomenon of fatigue failure, which occurs due to plastic deformation. By investigating the plasticity under cyclic loading, a deeper understanding of material behavior can be developed, and the factors that contribute to failure in structures can be identified. There are various models available to describe plasticity, including the bilinear, multilinear, and nonlinear hardening models. The elastic region, characterized by Hooke's law, provides a clear definition. Among these models, the multilinear and nonlinear models offer a more realistic representation of material behavior. However, a universally valid and accurate mathematical model for all materials remains elusive, as evidenced by the lack of a standard model that can predict the response of diverse materials [24]. The bilinear hardening model's unrealistic nature is counterbalanced by its simplicity and the ease with which it can be validated, rendering it an excellent candidate for use in numerical studies. In the context of cyclic loading, the behavior of the yield surface can be identified through the plasticity settings of isotropic hardening and kinematic hardening models.

The resulting models can be represented graphically as in Figures 3 and 4. Figures 3(a) and 3(b) illustrate the material yield surfaces based on isotropic and kinematic hardening models, highlighting the differences in plastic deformation behavior. Correspondingly, Figures 4(a) and 4(b) show the uniaxial bilinear stress–strain responses under the same hardening assumptions, providing a comparative view of the material's mechanical response. Ghadami *et al.* [25] employed a material mathematical model based on the Ramberg–Osgood approach and a plasticity model incorporating isotropic hardening. The findings indicated a notable degree of precision in the depiction of the behavior of short links composed of low-yield-point (LYP) steel. Numerous numerical investigations have utilized various plasticity models in their analysis of EBF structures. These include isotropic hardening, nonlinear kinematic hardening [22], multi-linear kinematic hardening [21], and combined models [5], [26].

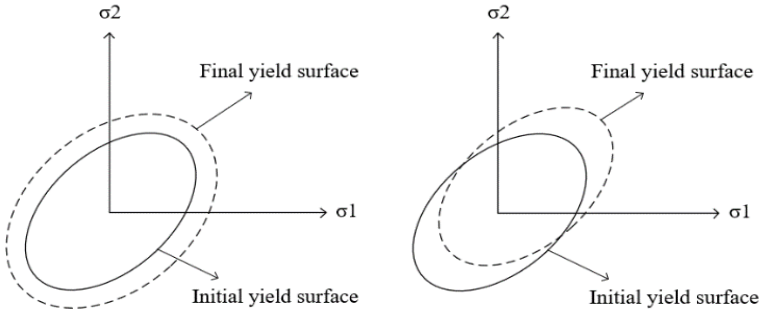

(a) (b)

Figure 3. Representation of yielding at the material surface (a) isotropic and (b) kinematic [24]

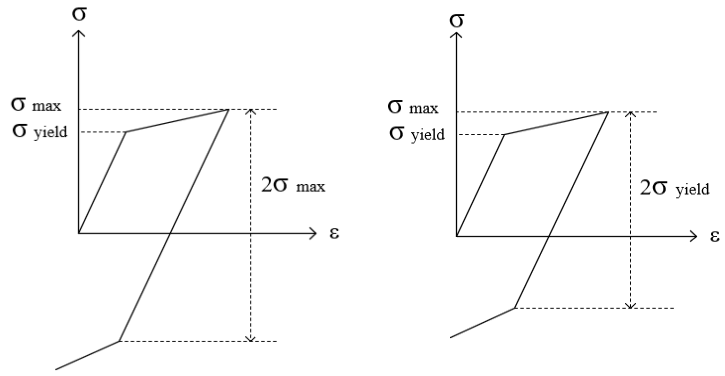

(a) (b)

Figure 4. Bilinear uniaxial stress-strain behavior of (a) isotropic and (b) kinematic hardening [24]

2.3. Test specimens

In this study, LCB link specimens were analyzed in accordance with the requirements of AISC 341-22. In order to see the comparison of the behavior and performance obtained, the analysis of the LCB links was carried out in two different classification models, namely, the difference in the mathematical model of the steel material and the plasticity model. The observed behavior is the critical strain position that causes buckling and fracture before and at the time of failure of the specimen. The position of the critical strain in LCB specimens is very important to observe whether the failure phenomenon occurs in the connecting beam or in the link. The specimen performance analyzed in these two specimen classification models are the shear strength and plastic rotation values achieved at failure. The test specimens comprised three pieces of LCB links, as delineated in Table 2. Figure 5 illustrates the structural configuration of the LCB within an EBF system. Figure 5(a) presents the overall K-braced EBF layout, whereas Figure 5(b) details the specific LCB configuration employed in the analytical investigation. The LCB, comprising coupled beams and links, is designed with a length that exceeds $2.6\,M_P/V_P$, while the links between the coupled beams are designed with a length that is less than $2.6\,M_P/V_P$. In the LCB model, the nominal shear strength of the coupled beams

(V_{n_CB}) is calculated based on the lowest value $(V_P, 2\,M_P/e)$, and the nominal shear strength of the links (V_{n_L}) is determined based on the lowest value $(V_P, 2\,M_P/e1)$. The values of plastic shear strength (V_P) and plastic moment (M_P) are calculated using the cross-sections of the coupled beams and links. The parameters of LCB length (e), link length (e1), and the nominal shear strength ratio for coupled beams and links are shown in Table 3.

Table 2. LCB link specimens

Test specimens	Stress-strain curve models		Plasticity models	
	Kauffman	Ramberg-Osgood	Multilinear kinematic hardening	Multilinear isotropic hardening
BU01	√	-	√	-
BU02	-	√	√	-
BU03	√	-	-	√

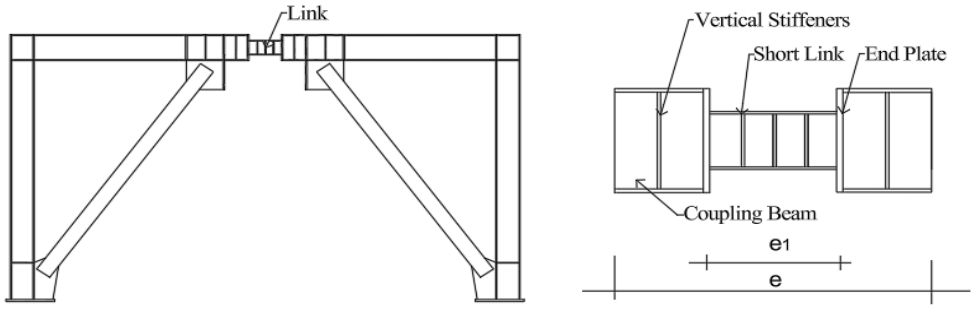

Figure 5. Configuration of the LCB testing specimen (a) the LCB of split k-braced configuration and (b) details of the LCB

Table 3. Properties of LCB link test specimens

Specimens	I-shaped sections		Properties of LCB			$\frac{V_{n-CB}}{V_{n-L}}$
	Link	Coupling beam (CB)	e (mm)	ρ	e_1 (mm)	
LCB	WF 200×100	WF 300×150	1,600	3.25	500	1.116

2.4. Boundary conditions

The boundary conditions were selected to replicate shear-dominated response of long links in EBFs while minimizing unintended axial forces. In accordance with approach outlined by Richards and Uang [27], one extremity of the linkage was subjected to complete restraint, prohibiting translation and rotation. Conversely, the opposing extremity was permitted translation exclusively in the transverse (shear) direction. All other degrees of freedom were restrained. This configuration ensures a nearly uniform shear force distribution along the link length and equal end moments under pure shear, with axial forces remaining negligible throughout the analysis. Sensitivity analyses confirmed that the presence or absence of axial restraint had no discernible influence on the hysteretic response, as shown in Figure 6. Hysteretic curves for models with and without axial force exhibited virtually identical strength, stiffness degradation, pinching, and energy dissipation characteristics. This insensitivity emerges due to the fact that long links exhibit minimal axial forces under the AISC 341-22 loading protocol when proper shear-dominant boundary conditions are enforced. The adopted boundary conditions provide a robust and realistic representation of isolated link behavior, thereby eliminating the artificial axial force effects commonly observed in earlier studies [28]. These conditions yield a consistent cyclic response that is independent of minor variations in end restraint. Consequently, these conditions were employed for all specimens reported herein. Theoretical and experimental evidence indicate that variations in boundary restraints, particularly the inclusion or exclusion of axial force, result in different strength ranges in link behavior. In models with axial restraint, the hysteretic response exhibits a slight positive slope, likely resulting from axial tension generated as a secondary effect of transverse loading. In contrast, the comparative model demonstrates stable and consistent hysteretic behavior, with similar trends observed regardless of the presence of axial force. It is noteworthy that the hysteretic curves for both restraint conditions are essentially identical, as illustrated in Figure 6. This conclusion is corroborated by comparisons between models with a fixed-end restraint and those with a free-end configuration, which confirm that axial restraint does not significantly influence the global hysteretic characteristics of the link.

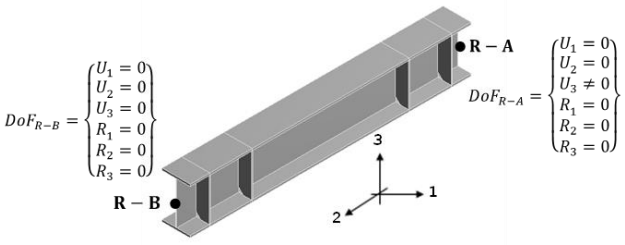

Figure 6. Boundary conditions

2.5. Loading protocol

The cyclic loading protocol was adopted from AISC 341-22 for long links. The loading process was meticulously regulated by the angle of link rotation, with incremental steps of 0.02 rad. Each amplitude up to 0.08 rad constituted a complete cycle, followed by three cycles at subsequent amplitudes, as delineated in the standard. Displacement-controlled boundary conditions were imposed at one end of the link while the opposite end was fully restrained, consistent with the shear-dominated response of long links in EBFs. To ensure numerical stability and accurate capture of post-yield behavior, each loading step comprised a minimum of 25 sub-steps, with automatic sub-stepping activated throughout the analysis.

3. RESULTS AND DISCUSSION

In addition to reporting the finite element results, the discussion as follows benchmarks the hysteretic features, overstrength, and plastic rotation capacity against prior experimental and numerical studies on EBF links to justify the observed trends. This study aimed to investigate the cyclic performance of long-LCB specimens in EBFs through nonlinear finite element analysis, with particular emphasis on the influence of the cyclic stress–strain formulation (mathematical model) and the plasticity model. Key response parameters—including hysteretic behavior, shear strength, overstrength ratio, and plastic rotation capacity—were evaluated and compared across the analyzed configurations.

3.1. Performance of numerical specimens

Figure 7 presents the shear force–link rotation hysteretic responses of the LCB specimens under cyclic loading. Figure 7(a) compares hysteretic behavior of specimens BU01 and BU02, whereas Figure 7(b) compares specimens BU01 and BU03. All specimens exhibited the characteristic shear-dominated behavior of long links in EBFs. Stable, full hysteretic loops were observed in the initial and intermediate cycles, indicating effective energy dissipation. Early cycles displayed nearly symmetric response and negligible stiffness degradation, consistent with uniform yielding along the link length. With increasing imposed rotation, progressive loop widening, reduced unloading stiffness, mild pinching, and moderate softening developed, reflecting the accumulation of plastic strains, onset of flange/web local buckling, and low-cycle fatigue effects typical of long links.

The progression from the initial stable hysteresis to the subsequent degradation of stiffness and pinching, ranging from mild to moderate, aligns with the extant experimental and numerical evidence on EBF links, particularly for intermediate-to-long links where strength degradation is governed by local flange/web buckling. A multitude of syntheses have previously indicated that link rotation capacity is contingent upon several factors, including link length ratio, loading history, section compactness, and web stiffening. For extended links, nonlinear finite element simulation can provide a reasonable estimate of rotation capacity because degradation is primarily buckling-driven rather than fracture-driven. A comparative evaluation of the three specimens was conducted, revealing distinct differences in strength, stiffness degradation, and energy dissipation capacity. It was observed that specimen BU03 produced the widest loops and the largest envelope curve. This specimen attained a peak shear strength of 391.86 kN and an overstrength ratio of 1.44. The specimen demonstrated the highest initial stiffness; however, pinching and stiffness deterioration became pronounced at lower rotation levels, consistent with it is reduced rotation capacity of 0.039 rad (195% of the AISC 341-22 minimum of 0.020 rad). In contrast, BU01 and BU02 exhibited peak shear strengths of 350.72 kN and 364.92 kN, respectively, resulting in overstrength ratios of 1.29 and 1.34. These specimens demonstrated enhanced stability, characterized by slower stiffness degradation and less severe pinching throughout the loading history. Their rotation capacities reached 0.051 rad and 0.050 rad (255% and 250% of the code requirement), respectively, thus exceeding BU03 by 30.8% and 28.2%.

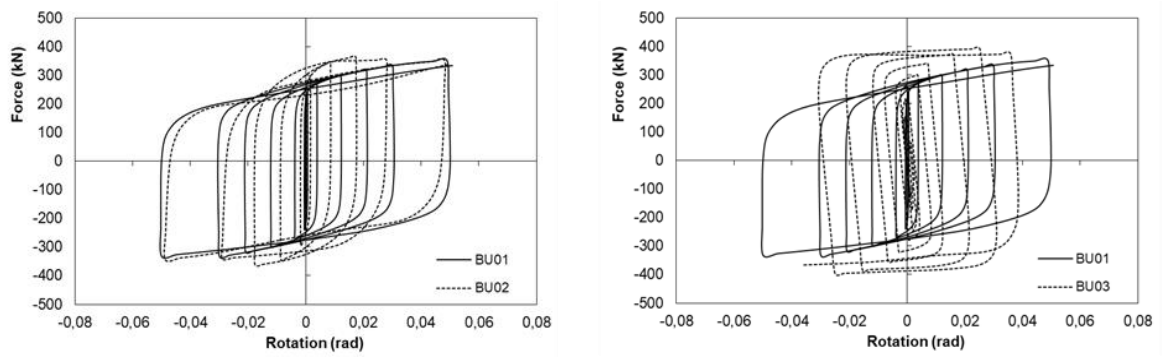

Figure 7. Shear force–link rotation hysteretic responses under cyclic loading: (a) comparison between BU01 and BU02 and (b) comparison between BU01 and BU03

Figure 8 illustrates the equivalent plastic strain (PEEQ) distributions of the tested specimens at link rotations of 0.01 rad and 0.05 rad. Figures 8(a) and 8(b) show the strain distributions of specimen BU01, Figures 8(c) and 8(d) correspond to specimen BU02, and Figures 8(e) and 8(f) represent specimen BU03. At a link rotation of 0.01 rad, plastic strains are primarily localized within the link region, indicating the initiation of inelastic deformation. As the link rotation increases to 0.05 rad, the plastic zone expands, and the strain concentration becomes more pronounced, reflecting the progressive development of yielding and damage accumulation under cyclic loading. In all specimens, the highest PEEQ remains concentrated within the link element, confirming that the intended energy dissipation mechanism is achieved while preventing excessive inelastic demand in the surrounding members.

These results highlight a clear strength–ductility trade-off that has also been reported for intermediate-to-long links: higher peak shear strength and initial stiffness can accelerate local flange/web buckling at larger rotations, reducing post-yield deformability [29], [30]. Similar long-link degradation mechanisms and rotation sensitivity to section compactness were documented in prior experimental and analytical studies [27], [31]. In this study, BU03 achieved the largest overstrength ($V_{max}/V_n = 1.44$) but the lowest plastic rotation (0.039 rad), whereas BU01–BU02 sustained larger rotations (0.050–0.051 rad) with moderate strength reduction. This pattern is consistent with the literature that identifies the timing and severity of local instability as key drivers of long-link ductility [32]. As established previously, the Kaufmann cyclic model combined with multilinear kinematic hardening most accurately reproduced the observed pinching, stiffness degradation, and cumulative energy dissipation. The consistent prediction of both strength- and ductility-dominated responses confirms the suitability of well-calibrated long-LCBs for seismic applications and provides a reliable analytical basis for optimizing link design and constitutive modeling in performance-based seismic engineering of steel EBF systems.

The location of the maximum PEEQ when yielding occurs in BU01 is in the link object between the coupling beams at the end of the link. In BU02 and BU03, the location of the maximum strain is also at the end of the coupling beam. The maximum PEEQ values obtained by the three specimens at a rotation angle of 0.05 rad were 0.04896 mm/mm for BU01, 0.7492 mm/mm for BU02, and 0.1664 mm/mm, respectively. The maximum PEEQ value obtained at a rotation angle of 0.05 rad, in consideration of the buckling phenomenon occurring in the uni specimen, serves to confirm the failure of BU03. The BU03 test specimens exhibited substantial buckling of the flange and web, as well as torsion of the test specimen, with strain values reaching the ultimate strain value based on the steel tensile test, as illustrated in Table 1. The maximum PEEQ achieved in test specimen BU02 has not reached the ultimate strain value based on the steel tensile test. The buckling phenomenon observable in the flange of the coupling beam did not, however, result in the failure of BU02 at the predicted rotation of 0.05 rad. The lowest maximum PEEQ was achieved by specimen BU01, and no buckling phenomenon was observed, in contrast to specimens BU02 and BU03. The maximum strain in specimen BU01 was observed at the ends of the links between the coupling beams, which differs from the location of the maximum strain observed in specimens BU02 and BU03. The maximum strain value observed in BU01 is lower than that predicted by the ultimate strain values derived from the tensile testing results, as shown in Table 1. Based on the observation of strain values and the failure to observe buckling, it can be predicted that the BU01 test specimen has not yet failed. Based on the maximum strain value and the occurrence of buckling, the failure of the test specimens commenced with BU03, BU02, and BU01, respectively.

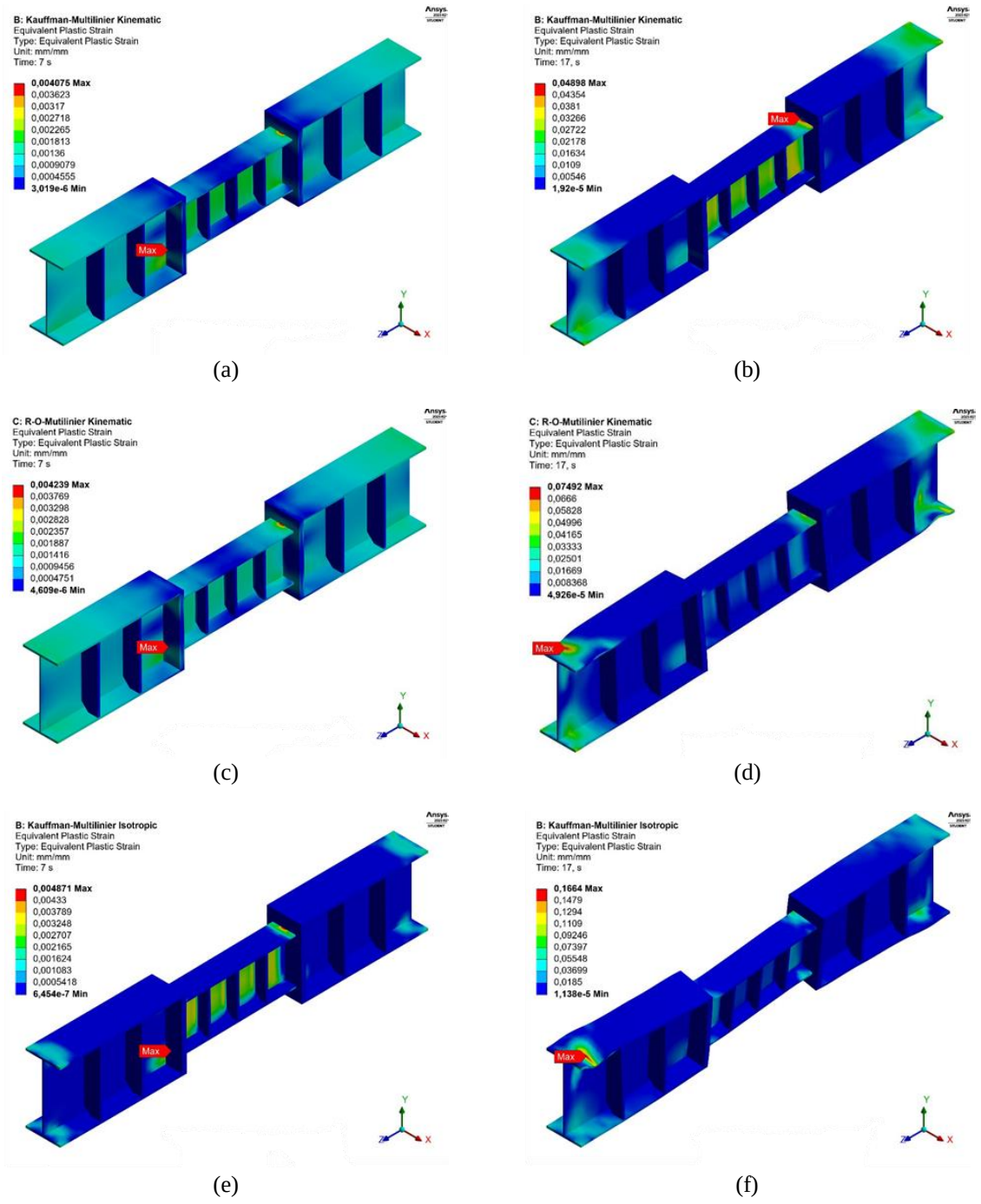

Figure 8. PEEQ of specimens: (a) BU01, rotation of 0.01 rad; (b) BU01, rotation of 0.05 rad; (c) BU02, rotation of 0.01 rad; (d) BU02, rotation of 0.05 rad; (e) BU03, rotation of 0.01 rad; and (f) BU03, rotation of 0.05 rad

3.2. Strength, overstrength, and plastic rotation

Table 4 summarizes the cyclic response of the three LCB specimens. All specimens significantly exceeded the nominal shear strength of 271.98 kN, attaining peak values of 350.72 kN (BU01), 364.92 kN (BU02), and 391.86 kN (BU03). The corresponding overstrength ratios were 1.29, 1.34, and 1.44, respectively. Specimen BU03 exhibited the highest shear resistance, surpassing BU02 and BU01 by 7.4% and 11.7%, respectively. The differences in peak strength between BU01 and BU02 were comparatively small (4.0%). Although BU03 achieved the greatest strength enhancement, its plastic rotation capacity was the lowest at 0.039 rad. In contrast, BU01 and BU02 reached 0.051 rad and 0.050 rad, respectively. These values represent 255%, 250%, and 195% of the minimum requirement of 0.020 rad specified in AISC 341-22

for long links. Consequently, BU01 and BU02 outperformed BU03 in rotation capacity by 30.8% and 28.2%, respectively. The results reveal a clear trade-off between strength and ductility. Higher shear overstrength in BU03 was accompanied by earlier onset of local buckling and reduced post-yield deformation capacity, whereas BU01 and BU02 provided greater inelastic rotation. This trade-off underscores the importance of selecting link geometry and material modeling parameters in accordance with the targeted seismic performance objectives—whether prioritizing energy dissipation through large plastic rotations or maximizing reserve strength against extreme seismic demands.

The obtained overstrength ratios $\left(\frac{V_{max}}{V_n=1.29-1.44}\right)$ should be interpreted in light of prior link research showing that overstrength depends on multiple factors (e.g., M–V interaction, flange contribution, and axial restraint effects) and cannot be represented by a single constant across link types. A comprehensive review indicates that $\Omega \approx 1.5$ is often a reasonable upper bound for links with $\rho > 1$, while design provisions adopt lower Ω values for economy in the capacity design of non-link members (e.g., $\Omega = 1.25$ for brace design in earlier AISC provisions). Consistent with AISC rotation limits reported in the literature (0.02 rad for long links in earlier editions), the plastic rotations achieved here (0.039–0.051 rad) exceed the code-based lower bound, and the differences among BU-series specimens are attributed to the onset and severity of local buckling that governs long-link degradation.

Table 4. Strength, overstrength, and plastic rotation of the specimens

No	Test Specimen	V_{max} (kN)	V_n (kN)	Over-strength (V_{max}/V_n)	Rotation (rad)	
					Req.	Test
1	BU01	350.72	271.98	1.29	0.020	0.051
2	BU02	364.92	271.98	1.34	0.020	0.050
3	BU03	391.86	271.98	1.44	0.020	0.039

4. CONCLUSION

Nonlinear finite element analyses of three AISC 341-22-compliant long-LCBs in EBFs demonstrated consistent reserve capacity under cyclic loading. The peak shear strengths achieved in this study ranged from 350.72 to 391.86 kN, indicating overstrength levels ranging from 1.29 to 1.44. Additionally, the plastic rotations recorded reached 0.039 to 0.051 rad, which exceeds the nominal shear strength of 271.98 kN and the 0.020 rad minimum threshold. Among the constitutive options, the Kaufmann cyclic model with multilinear kinematic hardening most accurately reproduced the hysteretic response (stiffness degradation, pinching, and energy dissipation); the mathematical stress–strain models remained stable, whereas isotropic and basic kinematic hardening introduced greater variability and unrealistic post-yield stiffness. A discernible strength-ductility trade-off was observed: BU03 exhibited the highest degree of overstrength, yet the lowest rotation, a consequence of earlier local buckling. Conversely, BU01 and BU02 experienced larger inelastic rotations, accompanied by only moderate strength reduction. The influence of link geometry and advanced cyclic constitutive representation on simulated seismic performance is significant, and the Kaufmann–multilinear kinematic combination is recommended for performance-based design and assessment of steel EBF systems, achieving a balance between reserve strength and deformation capacity.

ACKNOWLEDGMENTS

We would like to extend our sincere appreciation to Politeknik Negeri Lhokseumawe for providing their laboratory facilities as a research site.

FUNDING INFORMATION

The successful completion of this research endeavor would not have been possible without the facilitation and financial support provided by the leadership of the P3M unit at the Politeknik Negeri Lhokseumawe. We extend our profound gratitude to the leadership of the P3M unit at the Politeknik Negeri Lhokseumawe for their invaluable contributions.

AUTHOR CONTRIBUTIONS STATEMENT

This journal uses the Contributor Roles Taxonomy (CRediT) to recognize individual author contributions, reduce authorship disputes, and facilitate collaboration.

Name of Author	C	M	So	Va	Fo	I	R	D	O	E	Vi	Su	P	Fu
Musbar	✓	✓	✓	✓	✓	✓		✓	✓	✓			✓	
Hanif	✓	✓	✓	✓	✓		✓		✓	✓				✓
Khairul Miswar		✓				✓		✓		✓	✓	✓		

C : **C**onceptualization
M : **M**ethodology
So : **So**ftware
Va : **Va**lidation
Fo : **Fo**rmal analysis
I : **I**nvestigation
R : **R**esources
D : **D**ata Curation
O : Writing - **O**riginal Draft
E : Writing - Review & **E**diting
Vi : **Vi**sualization
Su : **Su**pervision
P : **P**roject administration
Fu : **Fu**nding acquisition

CONFLICT OF INTEREST STATEMENT

In the process of conducting research and preparing the manuscript, the authors declare no conflict of interest, either financially or personally.

INFORMED CONSENT

We have obtained informed consent from all individuals included in this study.

DATA AVAILABILITY

The data that support the findings of this study are available from the corresponding author, [M], upon reasonable request.

REFERENCES

[1] AISC, *Seismic provisions for structural steel buildings*. Chicago, United States: American Institute of Steel Construction, 2002.
[2] D. Dubina, A. Stratan, and F. Dinu, "Dual high-strength steel eccentrically braced frames with removable links," *Earthquake Engineering and Structural Dynamics*, vol. 37, no. 15, pp. 1703–1720, Dec. 2008, doi: 10.1002/eqe.828.
[3] X. Ji, Y. Wang, Q. Ma, and T. Okazaki, "Cyclic behavior of replaceable steel coupling beams," *Journal of Structural Engineering*, vol. 143, no. 2, Feb. 2017, doi: 10.1061/(ASCE)ST.1943-541X.0001661.
[4] M. Moestopo, D. Kusumastuti, E. Lim, U. Akbar, and M. S. Ramadhita, "Experimental study on the seismic behavior of replaceable shear links connected to coupling beam," *International Journal on Advanced Science, Engineering and Information Technology*, vol. 8, no. 2, Apr. 2018, doi: 10.18517/ijaseit.8.2.4323.
[5] M. Rahnemoun, S. K. Tabrizi, and P. Ashtari, "Experimental and numerical study on innovated steel shear resisting frame with haunched beams (SRFHBS)," *Journal of Constructional Steel Research*, vol. 197, Oct. 2022, doi: 10.1016/j.jcsr.2022.107495.
[6] M. B. Bozkurt and C. Topkaya, "Replaceable links with gusseted brace joints for eccentrically braced frames," *Soil Dynamics and Earthquake Engineering*, vol. 115, pp. 305–318, Dec. 2018, doi: 10.1016/j.soildyn.2018.08.035.
[7] Y. O. Özkılıç, M. B. Bozkurt, and C. Topkaya, "Mid-spliced end-plated replaceable links for eccentrically braced frames," *Engineering Structures*, vol. 237, Jun. 2021, doi: 10.1016/j.engstruct.2021.112225.
[8] M. B. Bozkurt, S. K. Azad, and C. Topkaya, "Development of detachable replaceable links for eccentrically braced frames," *Earthquake Engineering and Structural Dynamics*, vol. 48, no. 10, pp. 1134–1155, Aug. 2019, doi: 10.1002/eqe.3181.
[9] P. Mortazavi, O.-S. Kwon, and C. Christopoulos, "Seismic performance assessment of steel EBFS with conventional and replaceable yielding links designed with ASCE 7-16," *Journal of Structural Engineering*, vol. 150, no. 5, May 2024, doi: 10.1061/JSENDH.STENG-13093.
[10] P. Mortazavi, J. Binder, O.-S. Kwon, and C. Christopoulos, "Ductility-targeted design of cast steel replaceable modular yielding links and their experimental validation through large-scale testing," *Journal of Structural Engineering*, vol. 149, no. 7, Jul. 2023, doi: 10.1061/JSENDH.STENG-12097.
[11] P. Mortazavi, E. Lee, J. Binder, O.-S. Kwon, and C. Christopoulos, "Large-scale experimental validation of optimized cast steel replaceable modular yielding links for eccentrically braced frames," *Journal of Structural Engineering*, vol. 149, no. 7, Jul. 2023, doi: 10.1061/JSENDH.STENG-11633.
[12] F. Wang, T. Y. Yang, Y. Cui, and T. Chen, "Experimental and analytical study on the cyclic response of replaceable corrugated steel plate links," *Engineering Structures*, vol. 242, Sep. 2021, doi: 10.1016/j.engstruct.2021.112565.
[13] Z. Yao, W. Wang, C. Fang, and Z. Zhang, "An experimental study on eccentrically braced beam-through steel frames with replaceable shear links," *Engineering Structures*, vol. 206, Mar. 2020, doi: 10.1016/j.engstruct.2020.110185.
[14] H. Li, W. Zhang, and Q. Wei, "Seismic demand assessment on K-configuration eccentrically braced frames," *Structures*, vol. 45, pp. 1225–1238, Nov. 2022, doi: 10.1016/j.istruc.2022.09.096.
[15] X. Chen, S. Li, G. Liang, and M. He, "Numerical parameter analysis of high-strength steel frame with Y-eccentric brace using variable replaceable link," *Buildings*, vol. 14, no. 7, Jul. 2024, doi: 10.3390/buildings14072149.
[16] N. Mansour, C. Christopoulos, and R. Tremblay, "Experimental validation of replaceable shear links for eccentrically braced steel frames," *Journal of Structural Engineering*, vol. 137, no. 10, pp. 1141–1152, 2011, doi: 10.1061/(ASCE)ST.1943-541X.0000350.
[17] M. Lian and M. Su, "Seismic testing and numerical analysis of y-shaped eccentrically braced frame made of high-strength steel," *The Structural Design of Tall and Special Buildings*, vol. 27, no. 6, Apr. 2018, doi: 10.1002/tal.1455.
[18] K. G. Tan and C. Christopoulos, "Development of replaceable cast steel links for eccentrically braced frames," *Journal of Structural Engineering*, vol. 142, no. 10, Oct. 2016, doi: 10.1061/(ASCE)ST.1943-541X.0001550.

[19] Q. Shi, S. Yan, X. Wang, H. Sun, and Y. Zhao, "Seismic behavior of the removable links in eccentrically braced frames with semirigid connections," *Advances in Civil Engineering*, vol. 2020, no. 1, Jan. 2020, doi: 10.1155/2020/9405107.
[20] Z. Yin, D. Feng, and W. Yang, "Damage analyses of replaceable links in eccentrically braced frame (EBF) subject to cyclic loading," *Applied Sciences*, vol. 9, no. 2, Jan. 2019, doi: 10.3390/app9020332.
[21] Musbar *et al.* "Behavior of the link coupling beam on the eccentrically braced frame," *Journal of Southwest Jiaotong University*, vol. 58, no. 4, 2023, doi: 10.35741/issn.0258-2724.58.4.54.
[22] G. D. Corte and G. Cantisani, "FEM analysis of steel eccentric braces for seismic retrofitting," *Procedia Structural Integrity*, vol. 44, pp. 472–479, 2023, doi: 10.1016/j.prostr.2023.01.062.
[23] Musbar, B. Budiono, D. Kusumastuti, and H. D. Setio, "Behavior of modified long links with supplemental double stiffeners on eccentrically braced frames," *International Journal on Advanced Science, Engineering and Information Technology*, vol. 8, no. 6, pp. 2516–2524, 2018, doi: 10.18517/ijaseit.8.6.5852.
[24] R. R. Resapu and L. R. Perumahanthi, "Numerical study of bilinear isotropic; kinematic elastic–plastic response under cyclic loading," *Materials Today: Proceedings*, vol. 39, pp. 1647–1654, 2021, doi: 10.1016/j.matpr.2020.05.812.
[25] A. Ghadami, G. Pourmoosavi, and A. Ghamari, "Seismic design of elements outside of the short low-yield-point steel shear links," *Journal of Constructional Steel Research*, vol. 178, Mar. 2021, doi: 10.1016/j.jcsr.2020.106489.
[26] H. M. Moradi, B. H. Hashemi, and M. A. Jafari, "Experimental and numerical study on the cyclic behavior of link-beam shear-panel connected to frame beams," *Engineering Structures*, vol. 221, Oct. 2020, doi: 10.1016/j.engstruct.2020.111050.
[27] P. W. Richards and C.-M. Uang, "Effect of flange width-thickness ratio on eccentrically braced frames link cyclic rotation capacity," *Journal of Structural Engineering*, vol. 131, no. 10, pp. 1546–1552, 2005, doi: 10.1061/(asce)0733-9445(2005)131:10(1546).
[28] G. D. Corte, M. D'Aniello, and R. Landolfo, "Analytical and numerical study of plastic overstrength of shear links," *Journal of Constructional Steel Research*, vol. 82, pp. 19–32, Mar. 2013, doi: 10.1016/j.jcsr.2012.11.013.
[29] M. D. Engelhardt and E. P. Popov, "Experimental performance of long links in eccentrically braced frames," *Journal of Structural Engineering*, vol. 118, no. 11, pp. 3067–3088, Nov. 1992, doi: 10.1061/(ASCE)0733-9445(1992)118:11(3067).
[30] A. Daneshmand and B. H. Hashemi, "Performance of intermediate and long links in eccentrically braced frames," *Journal of Constructional Steel Research*, vol. 70, pp. 167–176, Mar. 2012, doi: 10.1016/j.jcsr.2011.10.011.
[31] T. Okazaki and M. D. Engelhardt, "Cyclic loading behavior of ebf links constructed of ASTM a992 steel," *Journal of Constructional Steel Research*, vol. 63, no. 6, pp. 751–765, Jun. 2007, doi: 10.1016/j.jcsr.2006.08.004.
[32] S. K. Azad and C. Topkaya, "A review of research on steel eccentrically braced frames," *Journal of Constructional Steel Research*, vol. 128, pp. 53–73, Jan. 2017, doi: 10.1016/j.jcsr.2016.07.032.

BIOGRAPHIES OF AUTHORS

Musbar is an associate professor in the Department of Civil Engineering, Politeknik Negeri Lhokseumawe, Indonesia. He received his bachelor's degree in Civil Engineering from Syiah Kuala University, Indonesia. His master's and doctoral degrees in civil engineering are from Bandung Institute of Technology, Indonesia. His research interests are in the areas of structural simulation and modeling, steel and concrete structures, and earthquake structures. He can be contacted at email: musbaribrahim@pnl.ac.id.

Hanif is an assistant professor in the Department of Civil Engineering, Politeknik Negeri Lhokseumawe, Indonesia. He received his bachelor's degree in Civil Engineering from Universitas Brawijaya, Indonesia, and his master's degree in Civil Engineering from Syiah Kuala University, Indonesia. His research interests include concrete materials and structures. He can be contacted at email: hanifts@pnl.ac.id.

Khairul Miswar is an associate professor in the Department of Civil Engineering, Politeknik Negeri Lhokseumawe, Indonesia. He received his bachelor's degree in Civil Engineering from Syiah Kuala University, Indonesia, and his master's degree in Civil Engineering from Universitas Gadjah Mada, Indonesia. His research interests include concrete materials and structures, structural simulation and modeling, and earthquake structures. He can be contacted at email: airolmiswar@gmail.com.